Journal Pre-proof

Antibacterial fluorescent carbonized polymer dots for directly dyeing silks at mild conditions

Zhao-Fan Wu , Xiao-Feng Shi , Xiao-Xiao Luo , Yu-Xuan Ji , Yuan-Qing Mao , Huan-Ming Xiong

PII: S1001-8417(26)00842-9
DOI: https://doi.org/10.1016/j.cclet.2026.113199
Reference: CCLET 113199

To appear in: *Chinese Chemical Letters*

Please cite this article as: Zhao-Fan Wu , Xiao-Feng Shi , Xiao-Xiao Luo , Yu-Xuan Ji , Yuan-Qing Mao , Huan-Ming Xiong , Antibacterial fluorescent carbonized polymer dots for directly dyeing silks at mild conditions, *Chinese Chemical Letters* (2026), doi: https://doi.org/10.1016/j.cclet.2026.113199

Antibacterial fluorescent carbonized polymer dots for directly dyeing silks at mild conditions

Zhao-Fan Wu [a,1], Xiao-Feng Shi [b,1], Xiao-Xiao Luo [a], Yu-Xuan Ji [a], Yuan-Qing Mao [b,*], Huan-Ming Xiong [a,*]

[a] *Department of Chemistry, Shanghai Key Laboratory of Electrochemical and Thermochemical Conversion for Resources Recycling, Fudan University, Shanghai 200438, China*

[b] *Shanghai Key Laboratory of Orthopaedic Implants, Department of Orthopedics, Shanghai Ninth People's Hospital, Shanghai Jiao Tong University School of Medicine, Shanghai 200011, China*

[1] Zhao-Fan Wu and Xiao-Feng Shi contributed equally to this work.

ARTICLE INFO

Article history:

Received

Received in revised form

Accepted

Available online

Keywords:

Carbonized polymer dots

Silk dyeing

Fluorescent fabrics

Antibacterial

Fluorescent surgical sutures

ABSTRACT

Three kinds of carbonized polymer dots (CPDs) with yellow, orange, and red fluorescence were synthesized under moderate conditions by tuning precursor structures. Unlike conventional silk dyeing processes that require mordants, fixing agents, or additional chemical grafting, these CPDs enable one-step simultaneous fluorescent dyeing and antibacterial functionalization of natural silk. The dyeing is achieved *via* simple aqueous immersion at room temperature, being compatible with the delicate silk fibers. These CPDs exhibited enhanced fluorescence emission in confined microenvironment, and were applied to dye natural silk fabrics directly, yielding multi-color fluorescent textiles with high retention rates (maximum 95 % for CPDs-3). Among them, the red fluorescent CPDs-3 could eradicate nearly 100 % of *Staphylococcus aureus* at a very low concentration of 50 μg/mL, retaining strong antibacterial activity on dyed silk. The silk stained with such CPDs were used as surgical sutures, which

* Corresponding authors.
E-mail addresses: MAOYQ1975@sh9hospital.org.cn (Y.-Q. Mao), hmxiong@fudan.edu.cn (H.-M. Xiong).

displayed the precise positions of the sutures through its bright red fluorescence.

The natural mulberry silk, due to its unique mechanical properties and excellent biocompatibility, has been used widely in biomedical fields including surgical sutures, wound dressings, and vascular stents [1–3]. *Staphylococcus aureus* (*S. aureus*), a prevalent wound pathogen, induces inflammation and causes persistent infection, delayed healing, and systemic complications [4]. Native silk fibroin lacks intrinsic antibacterial activity against *S. aureus* and spontaneous fluorescence, thereby requiring both antibacterial and fluorescent modification for practical biomedical applications [5–7]. To expand the functional versatility of silk fibroin materials, various functionalization strategies have been developed in recent years. One strategy focuses on the modification of pristine silk fibers, such as feeding silkworms with carbon dots/polymer dots to prepare fluorescent silk [8], or covalently grafting AIEgens onto silk fibers *via* click bioconjugation [9]. The other route relies on dissolving silk fibroin to fabricate regenerated materials including composite films, hydrogels, and multifunctional interfacial materials [10,11]. Such systems exhibit multi-signal responsiveness, self-healing, and self-adhesion properties, showing great potential in functional optical materials [12]. The former introduces specific single function on pristine silk fibers, while the latter achieves multi-functional integration *via* protein structural reconstruction. Therefore, achieving one-step integration of fluorescent and antibacterial functions while preserving the fiber morphology and intrinsic hierarchical structure of natural silk remains a challenge and worthy of exploration. Compared with the relatively low doping content of the silkworm-feeding strategy, direct aqueous dyeing of silk fibers is a facile and efficient alternative [13]. However, traditional fluorescent dyes and antibacterial agents require mordants, fixatives, low pH environments, and high-temperature treatment during modification, which inevitably damages the delicate structure of silk fibers and impairs their softness and mechanical toughness [14–16]. Furthermore, the stepwise modification processes tend to mutually interfere, weakening both fluorescent and antibacterial functions [17,18]. Therefore, it is necessary to develop a versatile dyeing agent with intrinsic luminescent and antibacterial properties that can tightly adhere to silk under mild conditions.

Carbonized polymer dots (CPDs) are a class of carbon-based nanoparticles with typical diameters of 1–10 nm, exhibiting excellent photoluminescence and biocompatibility [19]. Compared with highly graphitized carbon dots, CPDs synthesized from small-molecule precursors under mild conditions generally show lower carbonization degrees [20,21]. Their photoluminescence is predominantly governed by molecular-state emitters rather than well-developed carbon cores, which endows them with controllable surface states and

synthesis route endow CPDs with broad application prospects in lighting devices, fluorescent probes and biomedical fields [24]. Some CPDs possess inherent bioactivities, including favorable antibacterial, antioxidant, and anti-inflammatory capabilities [25–27]. Hence, it is feasible to fabricate CPDs with tailored surface states for tight binding to silk fibers, as well as tunable fluorescence and excellent antibacterial performance. However, related studies on fluorescent CPDs-dyed silk remain scarce, because typical CPDs generally exhibit low retention rates on silks after washing. Therefore, the fabrication of CPDs that integrate high fluorescence efficiency, robust antibacterial activity, and excellent dyeing fastness remains a considerable challenge.

In this study, four antibacterial organic conjugated molecules (Fig. 1, **a1**, **a2**, **b1**, **b2**) [28,29] were selected as precursors to fabricate CPDs *via* overnight heating in deionized water at 85 °C (detailed experimental methods are provided in Supporting information). The obtained CPDs-1, CPDs-2, and CPDs-3 emit brightly yellow, orange, and red fluorescence in viscous solvents like glycerol, respectively. More importantly, these hydrophobic precursors were transformed into CPDs with better water solubility and high adhesion to the natural silk. And their antibacterial abilities against *S. aureus* are much stronger than the precursors. After simple immersion in CPDs aqueous solutions, the silk fabrics were dyed stably, and exhibited bright colors in daylight and multi-colorful fluorescence under UV light respectively. CPDs-3 exhibits the best inhibitory effect against *S. aureus*, and this effect is inherited by the CPDs-3 stained silk. Using CPDs, one-step fluorescent staining and anti-*S. aureus* modification of silk are achieved *via* room-temperature aqueous immersion. The modified silk can be applied as surgical sutures, whose fluorescence allowed for the precise localization and visualization of the sutures on pig liver tissue and full-thickness skin wounds on black mice.

It is known that aromatic precursors can construct strongly fluorescent CPDs, particularly in the long-wavelength regions [30,31]. In the present work, salicylaldehyde derivatives (**a1**, **a2**) and indolium salts (**b1**, **b2**) were selected as precursors to produce CPDs with tunable fluorescence by adjusting the conjugated structure (Fig. 1) [32]. Since salicylaldehyde derivatives have intrinsic antibacterial activity against *S. aureus*, whose combination with indolium salts can produce CPDs with significant antibacterial performance toward *S. aureus* [33]. The formation processes for these CPDs are similar to those in previous reports [34,35], *i.e.*, phenolic hydroxyl groups can be oxidized by air to generate phenoxy radicals, which may polymerize to form polyphenol nanoparticles. Specifically, the reaction procedure may include the formation of aromatic fluorescent molecular intermediate from the precursors, localized condensation of these molecules to form conjugated aromatic clusters [36], and aggregation of these clusters driven by noncovalent interactions (π–π stacking and hydrogen bonding), leading to nanoscale assemblies [37,38]. It has been reported that, even at room temperature in air,

arc e

obtained CPDs are a hybrid system composed of molecular emissive centers, conjugated clusters and assembled architectures, stabilized through covalent linking and noncovalent interactions. With respect to our present samples, compared with CPDs-1, the conjugation degree of CPDs-2 is enhanced by replacing the indole ring with a benzo-indole ring in indolium salt precursors (from **b1** to **b2**, with **a1** unchanged); compared with CPDs-2, the conjugation degree is further enhanced by substituting the hydroxyl group at the 4-position on salicylaldehyde derivatives with a diethylamino group (a stronger electron-donating group, from **a1** to **a2**, with **b2** unchanged) [32]. Accordingly, the emission wavelengths of these CPDs are progressively redshifted. Although the as-prepared CPDs are dark powders with no fluorescence under UV light (Fig. S1 in Supporting information), their solutions in glycerol exhibit bright colors in daylight and tunable fluorescence under UV light (Fig. S2 in Supporting information). Synthetic reproducibility was evaluated by three parallel experiments, and the isolated product masses as well as average yields are listed in Table S1 (Supporting information). The average isolated yields of CPDs-1, CPDs-2 and CPDs-3 were determined to be 21.9 % ± 3.8 %, 45.6 % ± 8.0 % and 36.1 % ± 5.0 %, respectively.

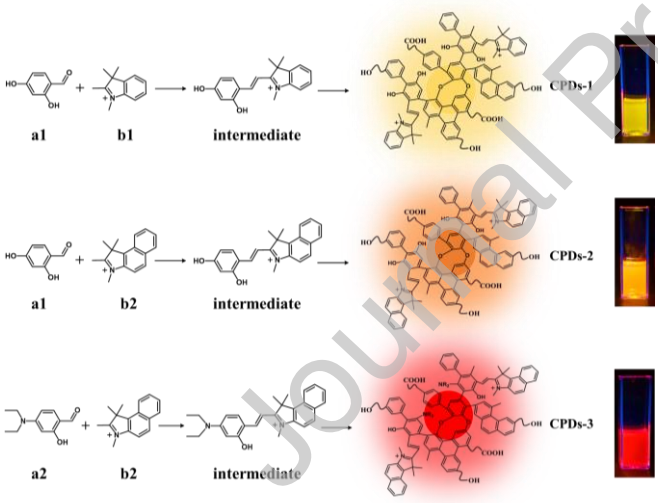

Fig. 1 Schematic illustration of the synthesis of CPDs-1–3 using different combinations of precursors (**a1**, **a2**, **b1**, **b2**). **a1**: 2,4-Dihydroxybenzaldehyde; **a2**: 4-Diethylaminosalicylaldehyde; **b1**: 1,2,3,3-Tetramethyl-3*H*-indolium iodide; **b2**: 1,1,2,3-Tetramethyl-1*H*-benzo[*e*]indolium iodide. The resulting CPDs show tunable fluorescence colors in glycerol under UV light, respectively.

The transmission electron microscopy (TEM) images (Figs. 2a–c) reveal that the as-prepared CPDs are monodispersed spherical nanoparticles, with weak lattice fringes of approximately 0.21 nm assigned to the (100) plane of graphitic carbon in their partially carbonized-like structure [42,43]. Particle size analyses (Fig. S3 in Supporting information) reveal that the three samples have average diameters of about 5.7, 5.5, and 7.5 nm,

res[illegible]n (500–1500 cm^{-1}, highlighted by the shaded area and green dashed box) of the precursors (**a1, a2, b1, b2**) shows well-resolved peaks, which become broadened and less-resolved in CPDs, indicating a structural transition from discrete small molecules to hybrid carbon nanostructures with diverse chemical environments [44]. Meanwhile, the aromatic C–H out-of-plane bending vibration of the indolium salt **(b1, b2)** at ~750 cm^{-1} (green arrows) decays or disappears in all three CPDs. The CPDs display a broad absorption band at 3200–3500 cm^{-1} assigned to O–H/N–H (the existing -OH/-NH-marked by orange arrows). The signals at about 1600 cm^{-1} and 1200–1300 cm^{-1} correspond to the conjugated C=C/C=N structures and the C–O–C vibrations, respectively [29]. These results verify the covalent coupling of aromatic rings and the extension of conjugated skeletons, further demonstrating that the CPDs are not simple aggregates of small molecules [45]. Notably, CPDs-1 and CPDs-2 exhibit stronger O–H/N–H signals compared with CPDs-3, consistent with the higher hydrophilicity of precursor **a1** relative to **a2**, and the correspondingly reduced water dispersibility of CPDs-3. All three samples show a broad XRD peak at 20°–25° (2θ) (Fig. 2g), indicating predominantly amorphous structures [46]. Raman spectra (Fig. 2h) show broad D (1350 cm^{-1}, disordered carbon) and G (1580 cm^{-1}, graphited carbon) bands, indicating the presence of a large amount of amorphous carbon. The G band of CPDs is usually attributed to the conjugated aromatic clusters and partially carbonized structure, rather than a well-defined graphitic core, and the decreasing I_D/I_G ratio suggests the enhanced conjugation [47]. XPS full spectra (Fig. 2i) reveal that these CPDs are composed of C, N, and O elements, with C being the most abundant and N being the least. In the fine spectra (Fig. S4 in Supporting information), the C, N, and O peaks are deconvoluted respectively, confirming the existence of -C–C/C=C (285 eV), C–O–C/C–N (286 eV), O–C=O (289 eV), C–N/C=N (400 eV), N–O/N^+ (403 eV), C=O (532 eV), and C–O–C (533 eV) [23,48]. The contents of each peak are listed in Table S2 (Supporting information). The high-resolution C 1s spectra confirm the coexistence of sp^2 and sp^3 hybridized carbon. With the increased proportion of surface C–O/C–N and N^+, the conjugation structure of CPDs is enlarged, the charge transfer is enhanced, and the excited state energy is decreased, leading to red-shift of fluorescence emission [34].

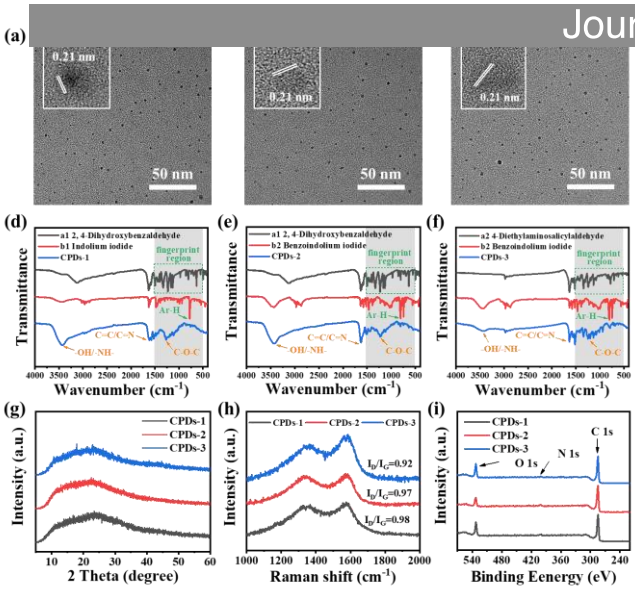

Fig. 2 TEM images and the inset HRTEM images of (a) CPDs-1, (b) CPDs-2 and (c) CPDs-3, respectively. (d–f) FTIR spectra of the precursors and corresponding CPDs. The shaded area with green dashed box highlights the fingerprint region (1500–500 cm^{-1}) of the precursors; green and orange arrows indicate characteristic peaks of the precursors and CPDs, respectively. (g) X-ray diffraction (XRD) patterns of CPDs. (h) Raman spectra of the CPDs, with the intensity ratios of the D/G peak (I_D/I_G). (i) Wide-scan XPS spectra of CPDs, respectively.

The absorption spectra of CPDs in Fig. S5 (Supporting information) show peaks in 200–300 nm are mainly attributed to $\pi \rightarrow \pi^*$ transitions of aromatic sp^2 domains. The peaks in 400–600 nm are attributed to the fluorescent groups, and their red-shifts are consistent with the fluorescent behaviors [49]. The fluorescence emission spectra (Figs. 3a–c) indicate CPDs have excitation-independent fluorescence emission peaks, with the maximum intensities at around 565 nm for CPDs-1, 585 nm for CPDs-2 and 605 nm for CPDs-3, respectively. Fig. S2 reveals that the glycerol solutions of these CPDs appear orange-red in daylight and exhibit yellow, orange, and red fluorescence under UV light, in accord with their absorption and emission spectra. The above results indicate that the fluorescence of CPDs is gradually red-shifted with the increased conjugation of precursors. Fig. S6 (Supporting information) displays UV-vis and fluorescence spectra of products from four single precursors. All differ from CPDs, verifying the formation of new materials. Moreover, the excitation-independent emission behaviors of our CPDs suggest that their luminescence mechanism is likely molecular-state emission [50,51]. Since the molecular-state emission can be effectively enhanced *via* hydrogen-bonding rigidification and restriction of intramolecular motions (RIM) [52], a high-viscosity solvent with abundant hydroxyl groups and moderate non-polarity can construct a hydrogen-bond crosslinked rigid microenvironment to suppress the intramolecular motions of organic fluorophores in CPDs and improve their fluorescence [53]. As a result, the fluorescence of our CPDs in water is weak, while their glycerol solutions show very strong emission.

excitation wavelengths, the fluorescence intensities of all samples increase with the glycerol content, till the maxima in the pure glycerol. Figs. 3g–i show dark-field images of the above samples at the same concentrations under UV light, consistent with the spectral results. Fluorescence spectra of CPDs samples dispersed in 50 % glycerol medium were measured at 5, 25, and 80 °C, respectively. As shown in Fig. S7 (Supporting information), PL intensity of CPDs-1–3 decrease with increasing temperature. To further decouple the coupled effects of solvent polarity, viscosity, and hydrogen-bonding capacity, fluorescence spectra of CPDs in nine solvents were measured under identical conditions, with related physicochemical parameters summarized in Table S3 (Supporting information). CPDs exhibited weak fluorescence in low-viscosity solvents with wide polarity ranges (1,4-dioxane, DMSO, formamide and water), indicating that polarity is not the dominant factor for fluorescence enhancement (Fig. S8 in Supporting information). In contrast, CPDs displayed significantly enhanced fluorescence in high-viscosity polyol solvents (EG, DEG, TEG, PEG300) with similar polarity and strong capability to form hydrogen-bonding networks. From EG to PEG300 with equivalent hydrogen-bonding confinement capacity, the FL intensity steadily increases with elevated viscosity, confirming that higher viscosity dominates the fluorescence enhancement under stable hydrogen-bonding networks. Based on the above results, the CPDs are speculated to consist of partially carbonized cores, polymerized aromatic clusters, and abundant surface functional groups (-OH, -COOH, $-NR_2$, *etc.*). Quaternary ammonium fluorophores are located in CPDs, for the N^+ signals are observed in the high-resolution XPS N 1s spectra of all CPDs. When the CPDs are surrounded in a dense viscous solvent with strong hydrogen-bonding interactions (*e.g.*, in glycerol), the intramolecular rotation and vibration of the fluorophores are effectively restricted, non-radiative decay pathways are suppressed, and thus the fluorescence emission is significantly enhanced [54]. The sequentially increased fluorescence intensity from DMSO to EG and PEG demonstrates that hydrogen-bonding confinement and high viscosity synergistically construct rigid microenvironments to boost CPDs fluorescence *via* the RIM mechanism, whereas solvent polarity plays a minor role.

To further verify the RIM mechanism, fluorescence lifetime and relative fluorescence quantum yield (RFQY) of CPDs in water and glycerol were measured. As shown in Table S4 and Figs. S9a–c (Supporting information), CPDs in water exhibited picosecond-scale lifetimes with unsatisfactory fitting results ($\chi^2 > 1.4$), while CPDs in glycerol presented valid lifetimes of 1.13–2.06 ns within the typical range for molecular-state emissive CPDs ($\chi^2 \leq 1.2$) [55]. The RFQY results are summarized in Figs. S9d–f and Table S5 (Supporting information), and the intuitive bar graphs in Fig. S10 (Supporting information) demonstrate that the quantum yields of all CPDs in glycerol are over ten-fold higher than those in water. The prolonged fluorescence lifetime and greatly improved

RF[illegible]y

suppresses non-radiative decay and enhances fluorescence emission efficiency. These photophysical results are consistent with the solvent-dependent experiments, further verifying the synergistic hydrogen-bonding confinement and viscosity-induced RIM mechanism. However, in the solid state, the observed fluorescence quenching is presumably attributed to strong π–π stacking between CPDs, which corresponds to aggregation-caused quenching (ACQ) [56,57]. To test the photostability of CPDs, the samples are irradiated continuously by different excitation light, respectively. After 1 h of irradiation, their fluorescence intensities decreased to 75 %, 87 %, and 86 % of the initial values for CPDs-1–3, respectively (Fig. S11 in Supporting information).

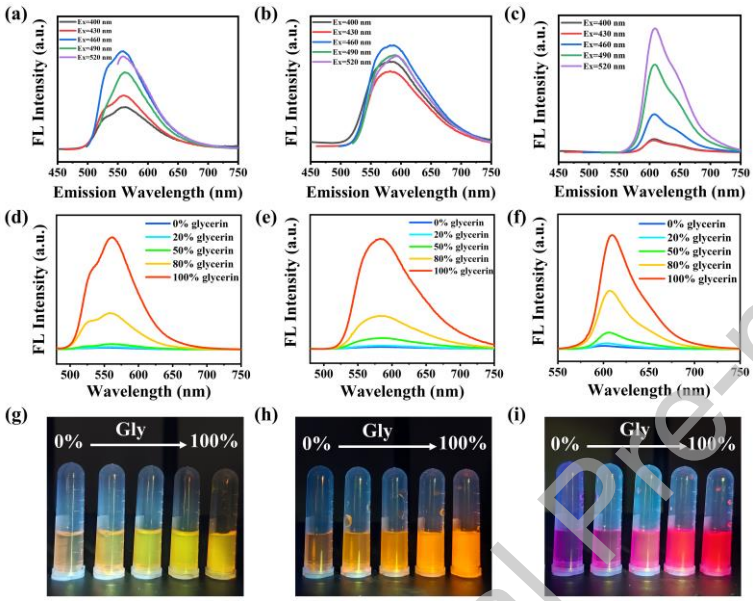

Fig. 3 Emission spectra of (a) CPDs-1, (b) CPDs-2, and (c) CPDs-3 in glycerol, excited by different wavelengths of light, respectively. (d–f) Fluorescence emission spectra of the three CPDs measured in aqueous solutions with different glycerol contents (0 %, 20 %, 50 %, 80 %, and 100 %), demonstrating a gradual increase in fluorescence intensity with increasing viscosity and hydrogen-bonding strength. Photographs of the CPDs solutions (0–100 % glycerol) under (g, h) daylight, and (i) UV irradiation, respectively.

As a type of nano fluorescent dyes, CPDs-1–3 can overcome the limitations of many organic molecular dyes, including poor water solubility, low photobleaching resistance, environmental pollution, and the damage to the silk from the indispensable organic solvents [58,59]. Their zeta potentials are +12.8, +15.2, and +24.5 mV, respectively (Fig. 4a), which are beneficial to dyeing silks. The natural white silk fabrics were dyed *via* immersion in the aqueous solutions of these CPDs (Fig. 4b), obtaining bright yellow, orange and red fluorescent silk fabrics, respectively. To find the optimal conditions, these silk fabrics were immersed in the solutions with different concentrations of CPDs, pH values and time, respectively (Figs. S12-S14 in Supporting information). According to the fluorescence brightness under UV light, the optimal conditions for subsequent experiments were

of 6 h. Afterwards, the fabrics were washed with 20 mL of water ultrasonically for 10 min each time after dyeing, repeated for 10 times. In general, the loose dyes were mostly removed after 4 times of washing (the photos of the cleaning solution are shown in Fig. S15 in Supporting information), while the remained CPDs kept stable in the fabric. Bright-field and dark-field photographs of dyed silk fabrics before and after cleaning are presented in Fig. 4c. The absorption spectra of CPDs solutions before/after dyeing and the first five washing solutions were recorded, respectively (Fig. S16 in Supporting information). When the absorbance exceeded the reliable range, the dyeing solutions were diluted by 20-fold prior to measurement, while the others were tested directly. Based on the results in Fig. S16, the optimal absorbance values are collected and the data are shown in Fig. S17 (Supporting information). Then, the retention rates of CPDs on silk fabrics were calculated according to Eq. S1 and Fig. S17 (Supporting information) [9], and the results are shown in Fig. 4d. All CPDs exhibit retention rates over 70 % after 10 times of washing. Particularly, CPDs-3 show a high retention rate of 95 %, indicating its stronger affinity to silks. The blue-emitting b-CDs and the green-emitting g-CDs with high quantum yield were synthesized respectively according to two recent reports, respectively [60,61]. Compared with Fig. 4c, fluorescence of b-CDs and g-CDs fabrics faded significantly after washing (Fig. S18 in Supporting information). Since the dyeing conditions were not precisely controlled, the calculation of retention rate for them was not performed further. The photostability and storage stability of CPDs-dyed silk fabrics were further investigated. After continuous irradiation with weak 365 nm UV light (12-16 W) for 9 days (Fig. S19 in Supporting information), no obvious color fading or fluorescence attenuation was observed. Fluorescence spectra collected at day 0, 3, 6 and 9 (Figs. S20a–c in Supporting information) showed minor fluctuations, implying that the samples possess favorable stability under ambient light and weak UV irradiation. Upon exposure to the intense laser source of the fluorescence spectrometer for 1 h (Figs. S20d–f in Supporting information), the fluorescence intensities of fabrics retained 86 %, 90 % and 97 % of their initial values, respectively. The CPDs-dyed fabrics exhibit better anti-photobleaching ability than pure CPDs samples (Fig. S11), and can basically meet the requirements for practical use and storage of fluorescent threads and fabrics. In Figs. 4e and f, the commercial white silk thread was stained with the above CPDs by the immersion method, and bright fluorescent patterns were sewn on the white silk cloth, demonstrating the practical application potential of CPDs in multicolor fluorescent textiles. In Fig. 4f, the white silk cloth was cut into letter patterns and then dyed with b-CDs, g-CDs, and CPDs-1–3 to produce a fluorescent pattern of "FUDAN".

The bonding effects of CPDs with silks mainly originate from hydrogen bonds and electrostatic attractions [9,62]. On one hand, the mild dyeing conditions in water and high retention rate are attributed to the

am s

with the –OH, $–NH_2$ on the silk surface, while the lipophilic parts enable CPDs to bind more readily to the lipophilic region of silk (like the part of *β*-sheet conformation) [63,64]. On the other hand, the high retention rate is ascribed to the positive Zeta potential of CPDs (Fig. 4a). The isoelectric point (pI) of silk fibers is approximately 4.5, which means their surfaces will carry negative charges when immersed in water (pH 5.5, owing to CO_2 dissolution from air), and thus the silk is apt to bind with our CPDs *via* electrostatic attractions [65]. From CPDs-1 to CPDs-3, the lipophilicity of their precursors increases due to the gradually increased aromatic rings and hydrophobic chains, leading to a gradual increase in their hydrophobic interactions to the silk [66,67]. Their higher fluorescence emission on the fabric than that in aqueous solution may originate from the same mechanism in glycerol. After dyeing and drying, CPDs form a dense hydrogen-bonding network with silk fabric, and silk establishes a rigid confined microenvironment, which restricts the molecular motion of fluorophores on CPDs and hinds the nanoparticle aggregation, leading to the stronger fluorescence emission.

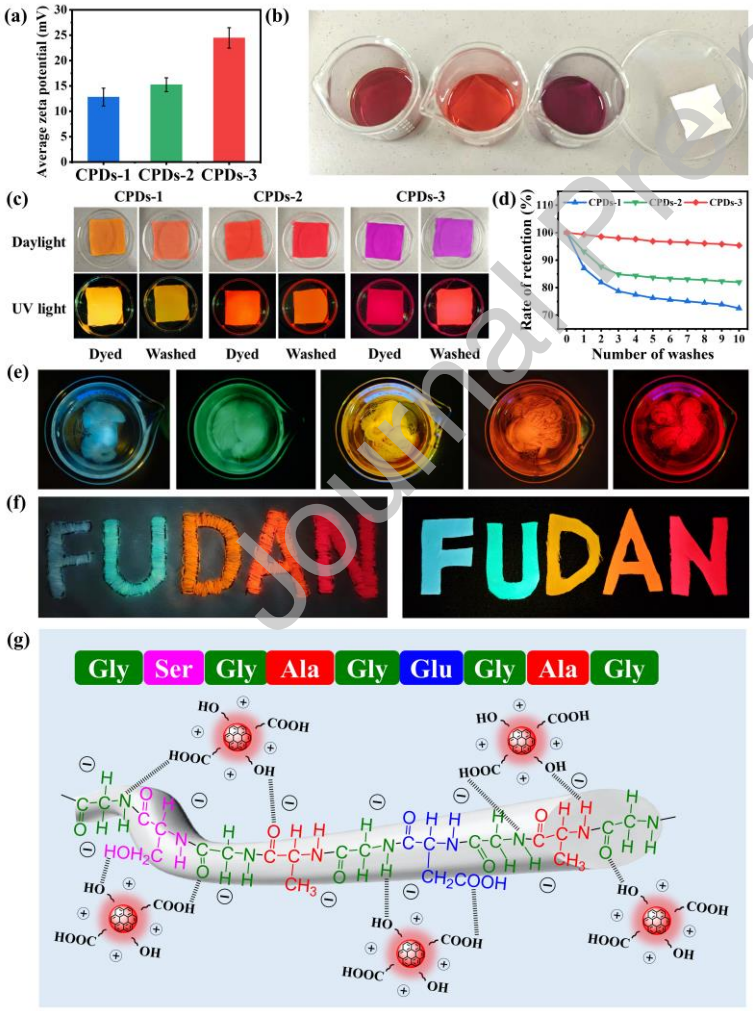

Fig. 4 (a) The average zeta potential of CPDs. (b) The 3 × 3 cm white silk cloth and those soaked in the aqueous solutions of CPDs-1–3, respectively. (c) Photos of the dyed silk cloths before and after 10 times of washing, under an incandescent lamp and a UV lamp, respectively. (d) Rates of retention calculated for different CPDs on silk

fab[illegible]n aqueous solutions of b-CDs, g-CDs (prepared according to other reports), and CPDs, respectively. (f) Photographs under UV lamp of the letter patterns sewn with the above dyed silk threads on a white silk cloth and the letter patterns of the dyed silk fabrics. (g) Schematic diagram of the binding mechanism (hydrogen bonds and electrostatic attractions) between CPDs and silk fibroin.

The spread plate method was employed to evaluate the antibacterial activity of CPDs against *S. aureus*, a common pathogenic bacterium that is prone to causing postoperative wound infections in clinical practice [68]. *S. aureus* was inoculated at the same concentration into petri dishes with and without CPDs1–3, respectively. As shown in Fig. 5a, all three kinds of CPDs exhibited antibacterial activities, and the bacterial counts decreased progressively with the increase in the concentration of CPDs. Quantitative analyses on bacterial colonies are presented in Fig. 5b. After co-cultivation with bacteria at 500 μg/mL, both CPDs-1 and CPDs-2 reduced the bacterial survival rate to about 40 %. CPDs-3 exhibited the highest bactericidal efficiency, with the bacterial survival rate approaching 0 % from the concentration of 50 μg/mL. To elucidate the differences, the antibacterial activities of the four CPDs precursors were evaluated. As shown in Fig. S21 (Supporting information), no significant difference in bactericidal activity was observed among the other three precursors (**a1**, **b1**, **b2**), whereas precursor **a2** (4-diethylaminosalicylaldehyde) showed a remarkable deviation, reducing bacterial survival to 30 % at 50 μg/mL (Fig. S21b). According to literature, this phenomenon is likely due to the diethylamino group on the benzene ring, which enhances bacterial adhesion and membrane disruption [69]. Among CPDs-1–3, only CPDs-3 was derived from precursor **a2**, which may account for its markedly higher antibacterial efficiency. In Fig. 5c, CPDs-1 and CPDs-3 show low cytotoxicity toward RAW264.7 cells, with ~80 % viability even at 500 μg/mL. CPDs-2 exhibits higher cytotoxicity, but cell viability remains ~90 % at 50 μg/mL. Considering the relatively low loading content and high retention rate of CPDs on dyed silk, it can be speculated that the dyed silk fibers possess favorable biosafety.

Based on the above findings, the antibacterial activity of CPDs-3-dyed silk was further evaluated by an *in vitro* experiment. In Fig. 5d, without silk, *S. aureus* rapidly proliferated 35 %, but when co-cultured with modified silk, even if it is only 40 mg, the bacterial count decreased to approaching 0 %. These indicate that unmodified silk lacks inherent antibacterial activity and may even serve as a favorable breeding ground for bacterial proliferation. In contrast, CPDs-3-dyed silk inherits the strong antibacterial activity of CPDs-3. Since the CPDs-3-dyed silk fabrics were subjected to 10 times of ultrasonic washing prior to bacterial co-incubation, and as

sug y

low. The antibacterial effect is thus more likely attributed to direct contact between the bacteria and the silk, which is beneficial for the clinical application of antibacterial fibers. The conventional black clinical surgical sutures are not visible under the dim light, making them difficult to discern in delicate surgeries. As a proof-of-concept validation, CPDs-dyed silk was used as fluorescent surgical sutures for porcine liver and black mice. All mice experiments were performed in accordance with the Guidelines for Care and Use of Laboratory Animals of Shanghai Jiao Tong University School of Medicine and the national guidelines of China. The experiments were approved by the Animal Ethics Committee (Animal Research Committee) of the Ninth People's Hospital (Approval No. SH9H-2023-A91-1). As shown in Figs. 5e and f, silk sutures stained with CPDs-1–3 display distinct suturing details, including the knotting position, fiber terminals and suture stitch orientation of the threads under UV light, while these details cannot be seen on the porcine liver sewn by the common sutures. Bright yellow, orange, and red fluorescence facilitated observation of wound healing and scar recovery, and the combined use of three-color fluorescent sutures allows sutures at different sites to be distinguished, further enhancing surgical accuracy [70–72]. Furthermore, CPDs-3 dyed silk combines bright fluorescence with strong antibacterial activity, which not only offers the fine suturing condition but also help eliminate wound bacteria. To further evaluate the medical applicability of dyed silk threads, their mechanical properties (tensile strength, elongation at break and knotted tensile strength) were tested before and after CPDs treatment. The corresponding stress-strain curves are presented in Fig. S22 (Supporting information). The statistical data listed in Table S6 are visualized as bar charts in Fig. S23 (Supporting information). The dyeing process exerted little influence on the intrinsic tensile strength of silk threads, with variations within 4.8 % relative to the pristine samples. The knotted tensile strength of silk modified with CPDs-1 and CPDs-2 showed no obvious reduction, while CPDs-3 group experienced a strength decrease of approximately 25 %. A moderate decline in elongation at break was also observed for all CPDs-dyed samples. These phenomena are mainly attributed to the thick and dense deposition of CPDs on silk fiber surfaces. At this stage, the dyeing parameters were optimized to prioritize fluorescence and antibacterial properties, rather than tuning the loading amount for ideal mechanical performance of threads. These findings provide a clear route for further research: systematically adjusting the loading density and coating thickness of CPDs to achieve a balanced performance among fluorescence, antibacterial activity and mechanical integrity.

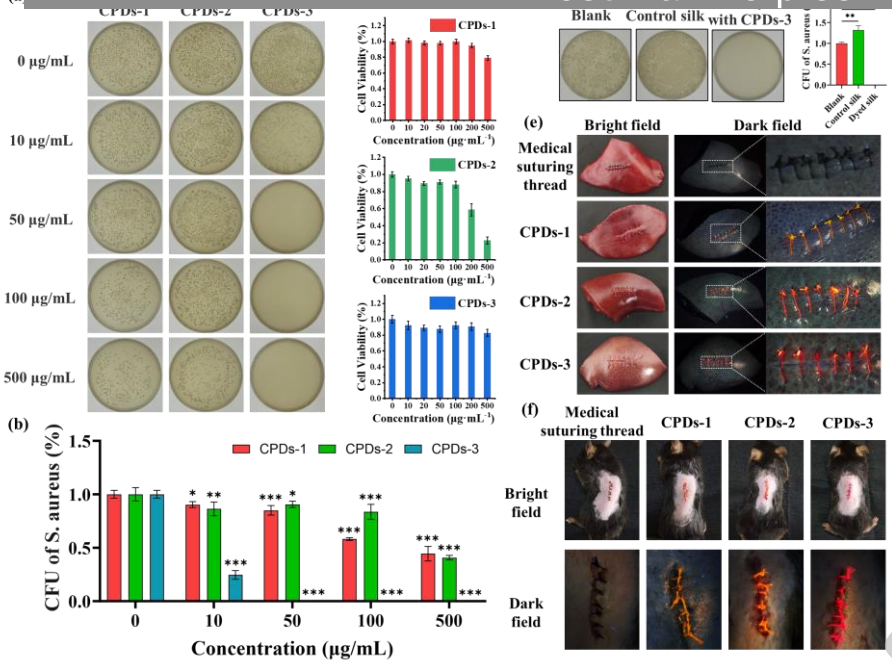

Fig. 5 (a) The effects of CPDs-1–3 of different concentrations when co-cultured with *S. aureus*. (b) Quantitative analysis of bacterial colony-forming units (CFUs). Data are presented as mean ± SD (n = 3). Significance levels: $P < 0.05$, $P < 0.01$, $P < 0.001$. (c) Cytotoxicity of CPDs against RAW264.7 cells measured by CCK-8 assay at different concentrations. Data are presented as mean ± SD ($n > 3$). (d) The antibacterial effect of silk fibers (40 mg) stained with CPDs-3 and quantitative analysis (n = 3). (e) Dark-field and bright-field photographs of pig liver wounds sutured with clinical surgical sutures and CPDs stained silk. (f) Photographs of full-thickness skin wounds (on the shaved dorsal) in 7–8-week-old black mice, sutured with clinical surgical sutures and CPDs-1–3 dyed silk.

In summary, this work presents a new route to synthesize CPDs with tunable fluorescence and varied antibacterial activities, which enables one-step dual-functionalization of silk with fluorescence and anti-*S. aureus* properties *via* simple aqueous immersion at room temperature without fixatives. Both fluorescence and antibacterial properties of CPDs are based on the reasonable selection of synthetic precursors. The yellow, orange, and red fluorescence of CPDs is adjusted by changing the conjugation degree. Although these precursors are hydrophobic, the as-prepared CPDs have rich water-soluble groups for their good dispersion in water. They can dye silk fabrics directly by a simple immersion with high retention rates, to produce bright multi-color fluorescent patterns on a large scale. More importantly, these CPDs are antibacterial, especially the optimal CPDs-3 that demonstrates excellent bactericidal activity against *S. aureus* at very low concentrations. The CPDs-3 dyed silks can be made into surgical sutures, which help surgical suturing by their bright fluorescence and antibacterial activity. Compared with studies that reconstruct silk fibroin into regenerated functional materials, this work focuses on direct modification of intact natural silk fibers. It complements the existing research system

of silk-based visual materials, and provides a simple and mild approach to prepare fluorescent silk textiles and biomedical sutures while preserving the inherent structure and basic mechanical properties of raw silk.

Declaration of competing interest

The authors declare that they have no known competing financial interests or personal relationships that could have appeared to influence the work reported in this paper.

Acknowledgments

This research was funded by National Natural Science Foundation of China (No. 22575057), Science and Technology Commission of Shanghai Municipality (No. 25ZR1401024), Shanghai Municipal Commission of Health and Family Planning (No. 2022JC031), and Shanghai Ninth People's Hospital Interdisciplinary Fund (No. JYJC202301).

References

[1] R. Zhang, Y. Zheng, T. Liu, et al., Chin. Chem. Lett. 33 (2022) 1599–1603.

[2] J. Wang, H. Liu, X. Shi, et al., Adv. Mater. 36 (2024) 2311593.

[3] K. Yang, J. Zhang, C. Zhang, et al., Chem. Soc. Rev. 54 (2025) 4973–5020.

[4] P. Lv, Y. Jiang, J. Wang, et al., Environ. Sci. Ecotechnol. 29 (2026) 100651.

[5] X.Q. Jin, J.L. Li, J. Liu, et al., Bioprocess. Biosyst. Eng. 48 (2025) 725–736.

[6] Z.F. Wu, Z.N. Sun, H.M. Xiong, Chin. J. Chem. 41 (2023) 2035–2046.

[7] K. Wen, C. Zhang, G. Zhang, et al., Adv. Mater. 36 (2024) 2314158.

[8] S. Fan, X. Zheng, Q. Zhan, et al., Nano-Micro Lett. 11 (2019) 75.

[9] C. Liu, H. Bai, B. He, et al., Angew. Chem. Int. Ed. 60 (2021) 12424–12430.

[10] E. Colusso, L. Cicerchia, M. Rigon, et al., J. Sol-Gel Sci. Technol. 107 (2023) 170–177.

[11] J. Li, Q. Ban, M. Xu, et al., J. Colloid Interface Sci. 691 (2025) 137455.

[12] M. Xu, J. Liao, J. Li, et al., Exploration 5 (2025) 270008.

[13] J. Li, Y. Li, S. Lu, et al., Adv. Fiber Mater. 4 (2022) 845–858.

[14] S. Guo, Y. Mu, J. Mu, et al., Bioresour. Technol. 437 (2025) 133142.

[15] X. Cheng, J. Hu, G. Wu, Appl. Surf. Sci. 717 (2026) 164780.

[16] Z. Lu, X. Wang, T. Zhang, et al., Chin. Chem. Lett. 31 (2020) 3139–3142.

[17] L. Zhou, K. Yu, F. Lu, et al., J. Clean. Prod. 243 (2020) 118604.

[18] Y. Song, J. Li, X. Li, et al., Interdiscip. Mater. 4 (2025) 927–940.

[19] X. Liu, G. Fan, Z. Liu, et al., Chin. Chem. Lett. (2026), https://doi.org/10.1016/j.cclet.2026.112620.

[20] S. Tao, T. Feng, C. Zheng, et al., J. Phys. Chem. Lett. 10 (2019) 5182–5188.

[21] B. Wang, G.I.N. Waterhouse, B. Yang, et al., Acc. Chem. Res. 57 (2024) 2928–2939.

[22] Q. Zeng, T. Feng, S. Tao, et al., Light: Sci. Appl. 10 (2021) 142.

[23] X. Niu, W. Zheng, T. Song, et al., Chin. Chem. Lett. 34 (2023) 107560.

[24] X. Li, C. Kang, S. Tao, et al., Carbon 237 (2025) 120122.

[25] B. Wang, G.I.N. Waterhouse, S. Lu, Trends Chem. 5 (2023) 76–87.

[26] M. Gao, S. Sun, H. Lin, et al., Chin. Chem. Lett. 37 (2026) 111055.

[27] F. Shan, T. Zhang, C. Liao, et al., Chin. Chem. Lett. 34 (2023) 108402.

[28] Z.F. Wu, X.X. Luo, X.F. Shi, et al., Nanoscale 17 (2025) 4958–4973.

[29] B.J. Wang, X.L. Jia, H.W. Sun, et al., Chem. Eng. J. 526 (2025) 170852.

[30] Y. Liu, H. Wang, S. Qu, Chin. Chem. Lett. 36 (2025) 110618.

[31] H. Ding, X.-X. Zhou, J.-S. Wei, et al., Carbon 167 (2020) 322–344.

[32] T. Han, Y. Wang, S. Ma, et al., Adv. Sci. 9 (2022) 2203474.

[33] X. Yuan, G. Du, Z. Wang, et al., Int. J. Biol. Macromol. 330 (2025) 148052.

[34] S. Tao, C. Zheng, B. Yang, Natl. Sci. Rev. 12 (2025) nwaf377.

[35] C. Xia, J. Zhong, X. Han, et al., Angew. Chem. Int. Ed. 63 (2024) e202410519.

[36] K. Lee, E. Park, H.A. Lee, et al., Nanoscale 9 (2017) 16596–16601.

[37] W. Wang, Z. Jia, Z. Deng, et al., Adv. Funct. Mater. (2026), https://doi.org/10.1002/adfm.202527665.

[38] Y. Ma, L. Wu, X. Ren, et al., Adv. Funct. Mater. 33 (2023) 2305867.

[39] J. Shi, S. Chang, Y. Gao, et al., Inorganics 12 (2024) 310.

[40] W.J. Zheng, Z.N. Sun, Y.M. Wang, et al., Nano Res. 17 (2024) 8495–8503.

[41] X. Wang, B. Yao, W. Song, et al., Chem. Eng. J. 520 (2025) 165821.

[42] D. Li, Z. Wang, S. Zheng, et al., Adv. Funct. Mater. 35 (2025) 2424929.

[43] J. Liu, T. Kong, H.M. Xiong, Adv. Mater. 34 (2022) 2200152.

[44] W. Hu, L. Li, X. Wang, et al., Chin. Chem. Lett. 36 (2025) 111612.

[45] Z. Ma, Y. Yu, S. Tao, et al., Polym. Sci. Technol. 1 (2025) 436–457.

[46] T.L. He, X.R. Zhang, Q.L. Ma, et al., ACS Appl. Energy Mater. 7 (2024) 5508–5516.

[47] C. Xia, S. Zhu, T. Feng, et al., Adv. Sci. 6 (2019) 1901316.

[48] Z.F. Wu, B.J. Wang, J.W. Ni, et al., Nano Lett. 24 (2024) 9675–9682.

[49] C. Li, J. Gao, S. Xiong, et al., Chem. Eng. J. 532 (2026) 174353.

[50] J. Bai, X. Wang, Y. Zhu, et al., Chin. Chem. Lett. 34 (2023) 107509.

[51] S. Zhu, Y. Song, X. Zhao, et al., Nano Res. 8 (2015) 355–381.

[52] Y. Liu, Z. Huang, X. Wang, et al., Adv. Funct. Mater. 35 (2025) 2420587.

[53] L. Wang, X. Liang, H. Chi, et al., Chin. Chem. Lett. 36 (2025) 110962.

[54] J. Cui, Y. Yao, C. Chen, et al., Chin. Chem. Lett. 30 (2019) 1071–1074.

[55] H. Ding, S.B. Yu, J.S. Wei, et al., ACS Nano 10 (2016) 484–491.

[56] C. Kang, S. Tao, F. Yang, et al., Aggregate 3 (2022) e169.

[57] X. Han, C. Xia, H. Wu, et al., Angew. Chem. Int. Ed. 64 (2025) e202422822.

[58] Y.Y. Zhu, J.J. Long, J. Clean. Prod. 399 (2023) 136632.

[59] T. Rasheed, TrAC, Trends Anal. Chem. 158 (2023) 116841.

[60] H. Ding, R. Zhao, Z.H. Zhang, et al., Chem. Eng. J. 476 (2023) 146405.

[61] Y. Liu, B. Wang, Y. Zhang, et al., Adv. Funct. Mater. 34 (2024) 2401353.

[62] Y. Shi, Q. Chang, T. Zhang, et al., J. Environ. Chem. Eng. 10 (2022) 108639.

[63] H. Xiao, T. Zhao, C.H. Li, et al., J. Clean. Prod. 165 (2017) 1499–1507.

[64] Md.R. Repon, B. Dev, M.A. Rahman, et al., Environ. Chem. Lett. 22 (2024) 1473–1520.

[65] J. Lu, Y. Zhou, Y. Zhou, Crit. Rev. Environ. Sci. Technol. 53 (2023) 1709–1730.

[66] W. Nie, J. Wu, J. Yang, et al., ACS Sustainable Chem. Eng. 11 (2023) 3873–3881.

[67] L.W. Jia, X. Zhang, ACS Appl. Nano Mater. 6 (2023) 1379–1385.

[68] H. Miao, P. Wang, M. Hu, et al., Chin. Chem. Lett. (2026) 112365.

[69] L. Chen, L. Wang, W. An, et al., Inorg. Nano-Metal Chem. 50 (2020) 872–879.

[70] D. Li, H. Shi, Q. Qi, et al., Adv. Sci. 10 (2023) 2303491.

[71] A.H. Ashoka, S.H. Kong, B. Seeliger, et al., Biomaterials 261 (2020) 120306.

[72] X. Chen, P. Tan, Y. Wen, et al., Chin. Chem. Lett. 31 (2020) 1499–1503.

Graphical Abstract

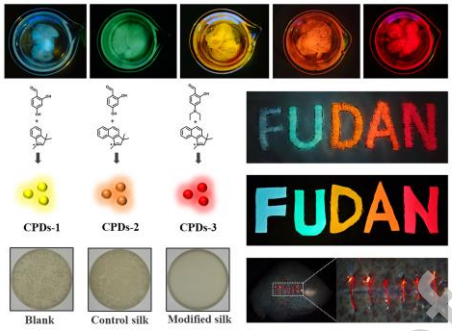

After careful selection of precursors, antibacterial carbonized polymer dots with tunable fluorescence are synthesized, which endow silk with dual functions of fluorescence and anti-*staphylococcus aureus* activity *via* one-step dyeing, forming colorful fluorescent patterns and surgical sutures for medical applications

Declaration of interests

☒ The authors declare that they have no known competing financial interests or personal relationships that could have appeared to influence the work reported in this paper.

☐ The authors declare the following financial interests/personal relationships which may be considered as potential competing interests: